

D3.1 Thermal shock on sealants

”Effects of Thermal Shocks on Integrity of Existing and Newly-Designed Sealants for CCS Applications”

CEMENTTEGRITY Deliverable 3.1, v. 1
Published 2023-04-01

Authors: Li, K., Pluymakers, A.
Rock Mechanics Lab, Delft University of Technology, the Netherlands

Reviewed by: Reinier van Noort (IFE Technology, Norway)

Keywords: *CCS, Well integrity, Sealants, Thermal shocks, Thermally-induced cracking*

Summary:

Sealants that can guarantee long-term wellbore sealing integrity are of great significance to the safe and sustainable storage of CO₂ in carbon capture and storage (CCS). In this study, we investigate how cyclic thermal shocks affect the integrity of four sealants of different compositions. These sealants include two reference OPC-based blends (S1 and S2), one newly-designed OPC-based blend that contains CO₂-sequestering additives (S3), and one calcium aluminate cement (CAC)-based blend designed for CCS applications (S4). We have conducted quenching and flow-through experiments to apply strong cyclic thermal shocks on samples of the four sealants, where we heated the samples to 120°C, and quenched them in, or flowed through water of 20°C. Using X-ray tomography (32 μm/voxel) before and after the experiment showed that both S1, S2 (reference OPC-based) and S4 (CAC-based) failed after thermal-shocking experiments. Cracks and new voids developed in the samples. Post-treatment strength testing shows that thermal shocks reduce the unconfined compressive strength of these three sealants. This implies that these compositions may not be optimal materials for long-term wellbore sealing during CO₂ injection and storage afterward. For all these three sealant compositions, quenching resulted in a greater reduction in strength (by 53% on average) than flow-through experiments (by 29% on average). On the contrary, we have not observed any cracks after either quenching or flow-through experiments in S3 sealant (OPC with CO₂-sequestering additives). We attribute the intactness of this sealant after thermal shocks to its higher thermal diffusivity than the other three sealants. Heat transfers more rapidly in this sealant and the associated thermal stresses are insufficient to cause any damage to its integrity, which makes this sealant a good candidate for wellbore sealing material that can effectively withstand strong thermal shocks encountered during CCS, though further studies are required.

Publication status:

A revised version of this article has been published in the *International Journal of Greenhouse Gas Control* Volume 133, March 2024, 104103, <https://doi.org/10.1016/j.ijggc.2024.104103>

1 Introduction

Carbon capture and storage (CCS), an technology to remove CO₂ from the atmosphere and store it in subsurface formations such as depleted oil and gas reservoirs or saline aquifers, has gained much attention in the last decades, as it contributes to fighting global climate change by reducing CO₂ emissions (Metz et al., 2005; Haszeldine, 2009; Selma et al., 2014; Budinis et al., 2018; Bui et al., 2018). The success of subsurface CO₂ storage depends on the permanent residence of CO₂ in the targeted reservoirs. However, during CCS, the periodic injection of pressurized cold CO₂ (Alnes et al., 2011; Eiken et al., 2011; Yoo et al., 2013; Samara et al., 2022) into warm reservoirs leads to strong cyclic thermal shocks. Under these temperature fluctuations, the wellbore and subsurface formations may undergo cyclic shrinkage upon injection of cold CO₂ and subsequent expansion after injection when the system equilibrates back to reservoir temperature. As a result, as shown in Figure 1, micro-annuli between wellbore casing, cement sheath, and wall-rock, and cracks in the cement may be induced (Carpenter et al., 1992; Carey et al., 2007; Roy et al., 2016; Vilarrasa and Rutqvist, 2017). The leakage of CO₂ through these pathways has been identified as one of the main challenges to securing safe and sustainable geological storage of CO₂ (Celia et al., 2005). Therefore it is of significance to understand how cement sheath integrity is affected by thermal cycling or shocks encountered in CCS.

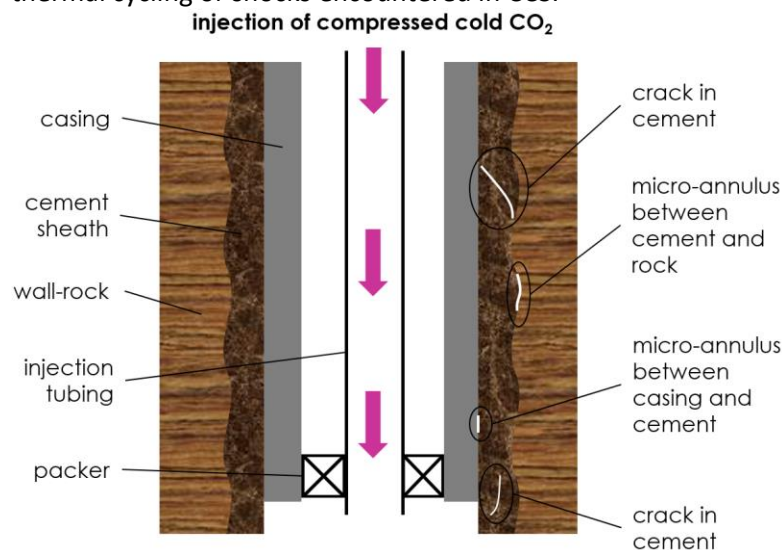


Figure 1: micro-annuli between wellbore casing, cement sheath, and wall-rock, and cracks in cement induced by injection of cold CO₂ and storage afterward.

In most depleted oil and gas wells targeted for CCS, ordinary Portland cement (OPC) is the main sealant composition, as it generally performs well as a zonal isolation material at relatively low costs in oil and gas industries (Parker et al., 2009; Santra and Sweatman, 2011; Lesti et al., 2013). However, the sealing integrity of wellbore using OPC-based sealant can be vulnerable and prone to deteriorate under strong temperature fluctuations during cyclic CO₂ injection and storage afterward. Albawi et al. (2014) conducted experiments with micro-computed tomography (micro-CT) to study the effects of thermal cycling on the integrity of a wellbore sample consisting of casing pipe, OPC-based sealant, and rock. Their sample was downscaled with a factor of 4 from a real wellbore section with a 311 mm borehole and 244 mm casing. They found thermal cycling at a temperature fluctuation amplitude of 75°C caused leakage pathways up to several millimeters thick by debonding at casing/cement and cement/rock interfaces. Lund et al. (2015) performed simulations by considering the thermal properties of casing, cement, and rock to model the study by Albawi et al. (2014). They concluded that the integrity of the sample under thermal cycling was

dependent on the thermal properties of all components of the sample. Large temperature fluctuations may lead to significant thermal stresses which could possibly damage the cement. De Andrade et al. (2015) also carried out experiments on a wellbore sample with the same configuration and dimensions as the one used by Albawi et al. (2014) to study the effects of thermal cycling. They concluded that shear failure was the most relevant mechanism for the debonding at interfaces. They further pointed out that, compared to sandstone, shale can better withstand thermal cycling, due to its higher stiffness and therefore greater resistance toward shear failures. All studies to date focused on integrity at the interfaces between casing, cement, and rock, while the integrity of the cement material itself when it undergoes thermal shocks remains unknown.

Besides OPC-based sealants, the efficacy of other alternatives under such temperature fluctuations is still unclear. Therefore, for future CCS wells, seeking improved wellbore sealing materials and testing their suitability to maintain enhanced long-term wellbore integrity is imperative. For example, calcium aluminate cement (CAC) becomes more and more popular, as it has a significantly higher early strength gain and a higher heat of hydration than OPC (Barborak, 2010). These characteristics make it attractive in the construction of future wells for CCS. Dugonjic-Bilic et al. (2011) tested the performance of a sealant composition based on CAC with a retarder in a CO₂ environment. They found that the ability of their composition to control water loss is suitable in CCS applications. However, how this sealant composition behaves under thermal cycling or shocks is still unknown.

In our study, we expose four sealant compositions, including existing and newly-designed OPC blends, and CAC blend, to strong cyclic thermal shocks by either quenching or flow-through experiments to study their integrity and suitability for CCS applications.

2 Experimental Materials, Apparatus, and Methodologies

In our study, two sample types are used: solid cylindrical samples (Φ3 x 7 cm) and samples of the same dimensions but with a Φ4 mm central borehole along the vertical axis. The latter mimics a sealant with a pre-existing leakage pathway. Sealant samples are of four different compositions (see Table 1), namely S1: standard OPC-based blend, S2: ultra-low permeability OPC-based blend, S3: OPC-based blend with CO₂-sequestering additives, and S4: CAC-based blend. These sealants include representatives of currently-used wellbore sealing materials in old oil and gas wells considered for CO₂ storage (S1 and S2, as references), and designed blends, targeted for newly drilled CCS wells (S3 and S4). Table 1 shows an overview of the four different sealant compositions and their respective technology readiness levels (TRL's).

Sealant	Composition	TRL
S1	1.90 SG class G cement with 35% BWOC silica flour	7: proven technology
S2	1.90 SG ultra-low permeability class G cement with 35% BWOC silica flour, with expansion agent in form of dead-burnt MgO	7: proven technology
S3	1.90 SG class G cement with 35% BWOC silica flour, with expansion agent in form of dead-burnt MgO, and CO ₂ -sequestering additives	3: prototype tested
S4	1.80 SG calcium aluminate cement-based blend	7: proven technology

Table 1: an overview of four sealant compositions and their TRL's.

For cementitious materials, it can take years to complete their strength-gaining process (Neville and Brooks, 1987). All samples used in this study are prepared by Halliburton AS Norway, in accordance with API specification 10B-2. This includes a water/cement ratio of 0.4, and curing at 150°C and 30 MPa for 28 days. The high temperature and pressure ensure that most chemical reactions have gone to near completion after curing, and as such it ensures that the mechanical and thermal properties of our samples will not vary significantly during the study duration. After curing, all samples are submerged in fresh water and stored at room temperature until use. In our study, all samples are completely dried before each experiment in an air-circulated oven (model UF75, Memmert). Samples are placed in the room temperature oven, and we first apply a ramping rate of 2.5°C/min to heat the sample to 80°C and leave the sample at 80°C for 2 days. After complete dewatering, we then cool the sample down to room temperature at the same ramping rate. These procedures ensure that associated thermal stresses during heating and cooling are minimum, and cause no damage to the integrity of the sample.

Before any thermal-shocking experiments, we determine the mechanical and thermal properties of the four sealants (Table 2). We perform unconfined compression tests to measure unconfined compression strength (UCS), Young's modulus, and Poisson's ratio of intact samples, both solid ones and those with a borehole. Mechanical testing is carried out using a 500 kN loading frame. Displacement is controlled with two high-precision linear variable differential transformers (LVDTs) with a 2 mm range, and on the sample a circumferential strain gauge is mounted with a 10 mm range. All UCS tests are carried out in displacement control mode with a ramping rate of 0.0005 mm/s, corresponding to a strain rate of 7.1×10^{-6} /s. Furthermore, we use a thermal constants analyzer (Hot Disk® TPS 2200) to measure the thermal conductivity and specific heat capacity of the sealants. The thermal diffusivity, a , which describes the ability of the sealant to conduct thermal energy relative to its ability to store thermal energy, can then be calculated by:

$$a = \frac{\lambda}{\rho c} \quad (Eq. 1)$$

where λ is the thermal conductivity of the sealant, ρ the density, and c the specific heat capacity.

Note that all properties of solid samples of each sealant composition listed in Table 2 are averaged based on measurements of three samples each made at an interval of one month. The relatively small standard deviation implies that our measurements are repeatable, and the mechanical and thermal properties of sealants have not changed throughout our study duration. The mechanical properties of samples with a borehole are almost the same as solid samples. This is probably because the borehole is too small compared to the sample, with a sectional area ratio of 1.8%, to substantially impact sealant mechanics. Table 2 also gives the permeability of the four sealants, provided by Halliburton AS Norway.

To quantify the effects of thermal shocks on the sealants, we use an X-ray micro-tomography (micro-CT) scanner (model Nanotom 180 NF, Phoenix X-ray Systems & Services GmbH) to scan samples at a voxel resolution of 32 μm . We then use Phoenix datos software (version 2.0, GE Measurement & Control solutions) to post-process the images and further use Avizo software (version 2020.2, ThermoFisher Scientific) to construct the 3D microstructure of cracks and voids in samples before and after experiments. The workflow of image analysis is detailed in the Appendix. In addition, we measure the UCS of samples after the experiments to study how these thermal-induced cracks and voids affect sealant integrity. Table 3 shows all samples to be tested and their respective experimental schemes.

Sealant	Unconfined compressive strength [MPa]	Young's modulus [GPa]	Poisson's ratio [-]	Thermal conductivity [W/(m·K)]	Specific heat capacity [J/(kg·K)]	Thermal diffusivity [mm ² /s]	Permeability [μDarcy]
S1, solid	98.57±1.10	13.52±0.26	0.157±0.002	0.82±0.04	878±18	0.492±0.008	0.14
S1, with borehole	99.82	13.44	0.143				
S2, solid	80.34±1.44	12.55±0.11	0.153±0.010	0.93±0.03	936±11	0.523±0.006	0.00005
S2, with borehole	81.14	12.03	0.162				
S3, solid	33.29±0.87	6.13±0.09	0.124±0.007	1.04±0.02	684±13	0.800±0.007	0.014
S3, with borehole	33.41	6.06	0.139				
S4, solid	35.30±1.42	6.52±0.05	0.157±0.013	0.89±0.02	970±21	0.510±0.006	0.32
S4, with borehole	34.26	6.58	0.172				

Table 2: mechanical and thermal properties as measured before thermal shocking, and permeability of the four sealants (provided by Halliburton AS Norway).

No.	Sample name	Sealant composition	Sample configuration	Experimental schemes
1	S1-1	S1, OPC blend	Solid	micro-CT → quenching → micro-CT → UCS
2	S1-2		With a borehole	micro-CT → flow-through → micro-CT → UCS
3	S1-3			
4	S2-1	S2, OPC blend with ultra-low permeability	Solid	micro-CT → quenching → micro-CT → UCS
5	S2-2		With a borehole	micro-CT → flow-through → micro-CT → UCS
6	S2-3			
7	S3-1	S3, OPC blend with CO ₂ -sequestering additives	Solid	micro-CT → quenching → micro-CT → UCS
8	S3-2		With a borehole	micro-CT → flow-through → micro-CT → UCS
9	S3-3			
10	S4-1	S4, CAC blend	Solid	micro-CT → quenching → micro-CT → UCS
11	S4-2		With a borehole	micro-CT → flow-through → micro-CT → UCS
12	S4-3			

Table 3: an overview of all samples to be tested and their respective experimental schemes. Quenching is type 1 testing, and flow-through is type 2 testing.

In our experiments, we adopt two experimental approaches to study the effects of thermal shocks on sealant integrity. We either quench pre-heated solid sealant samples (type 1) or flow cold water through the pre-heated samples with a central borehole (type 2). Figure 2 shows the procedure for the two approaches.

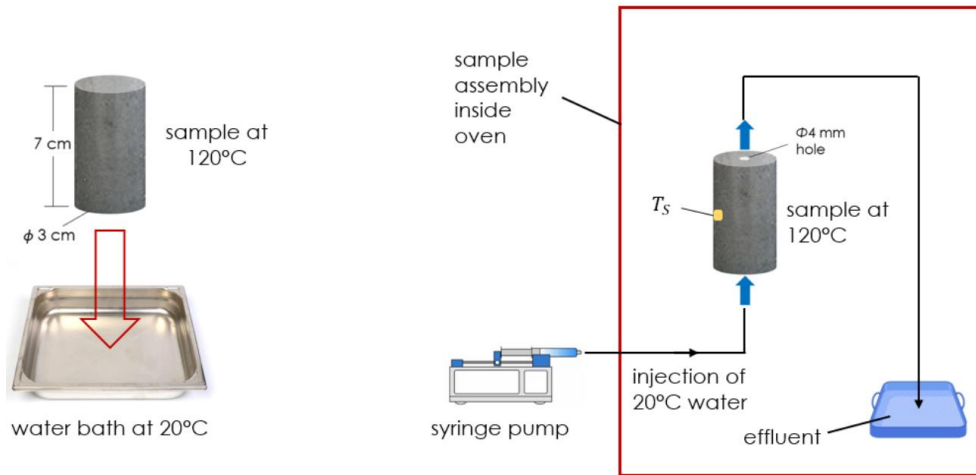


Figure 2 left: procedure for type 1 quenching experiments; **right**: procedure for type 2 flow-through experiments.

In type 1 quenching experiments, we first heat the sample to 120°C and maintain it at this temperature for half an hour in the oven, and then quickly transfer the sample into a 6 L 20°C cold water bath. After that, the sample is reheated to 120°C in the oven for the next shock. This is repeated eight times. These temperatures are representative for current CCS operations in reservoirs up to 3 km deep (Eiken et al., 2011; Lescanne et al., 2011; Yoo et al., 2013). For each sealant composition, we conducted quenching experiments on two samples separately, at an interval of three months.

In type 2 flow-through experiments, the whole sample assembly is placed in the oven at 120°C. After the assembly stays at this temperature for half an hour, we use a syringe pump (model 1000D, Teledyne ISCO) to inject 160 mL 20°C water through the sample in 2 minutes to apply the strongest thermal shock possible. We then halt for 12 minutes before the next injection to allow the sample to heat up again. As shown in Figure 1 (right), a thermocouple (type K, NI-9219, National Instruments, max. reading 700°C, accuracy $\pm 1^\circ\text{C}$) is mounted in the middle on the outer surface of the sample to measure the temperature, T_s , during the experiment. In type 2 experiments, we also performed eight cycles of thermal shock, and we tested one sample for each sealant composition.

In addition, we carry out reference experiments to investigate the effect of water exposure, by applying eight wet/dry cycles on one solid sample of each sealant composition. This allows us to examine how the process of repeated drying and wetting during both types of thermal-shocking experiments alone affects the sealant integrity. In each wet/dry cycling experiment, we first dry the sample at room temperature for 10 hours, then soak it in room temperature water bath for 2 minutes before the next drying, i.e. the equivalent of the quenching procedure, without the thermal effect. After the wet/dry cycling, we measure the UCS's of the four samples of different compositions.

3 Results

3.1 Effects of thermal shocks on the microstructure of sealant samples

Figures 3 to 6 show the microstructure of the two samples before and after type 1 quenching experiments for each of the four sealant compositions S1 to S4, respectively. These images show the structure of cracks and voids in samples, where interconnected cracks are displayed in the same color. The voids displayed

in samples of S1 and S3 compositions before quenching (Figures 3 and 5) are due to trapped air during cement casting. Note that samples of S2 and S4 do not have pre-existing voids, so orthogonal slices are given in Figures 4 and 6 to illustrate the intactness of the samples before quenching.

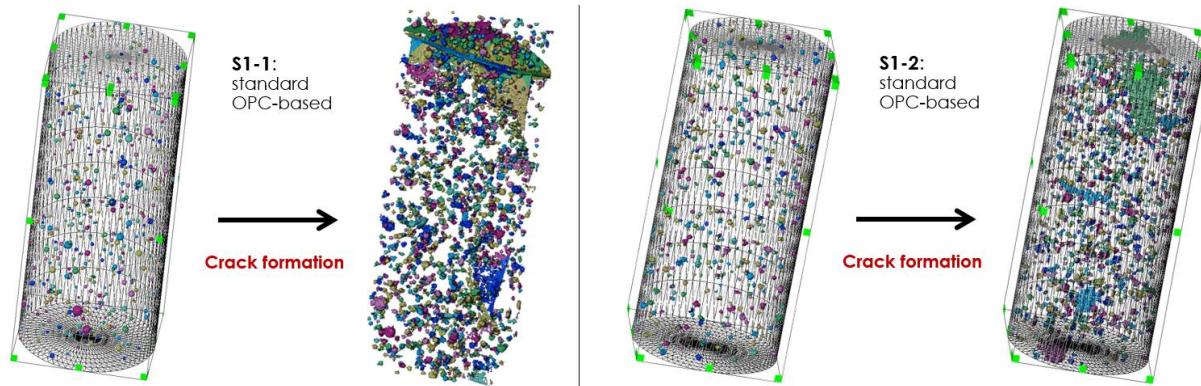


Figure 3: microstructure of samples S1-1(left) and S1-2 (right) before and after quenching. Voxel resolution of 32 μm . Samples are of sealant composition S1, standard OPC-based. Some connected cracks and many new voids develop in both samples.

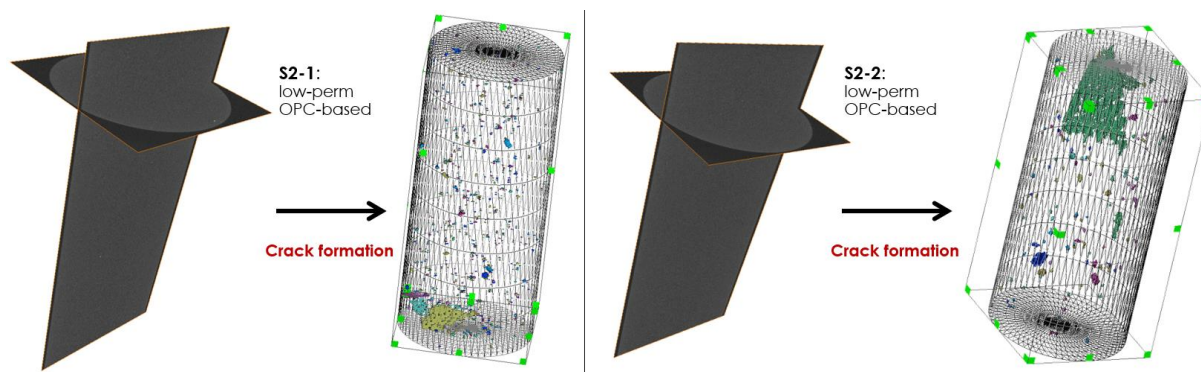


Figure 4: microstructure of samples S2-1(left) and S2-2 (right) before and after quenching. Voxel resolution of 32 μm . Samples are of sealant composition S2, low-permeability OPC-based. Some connected cracks and visible new voids develop in both samples.

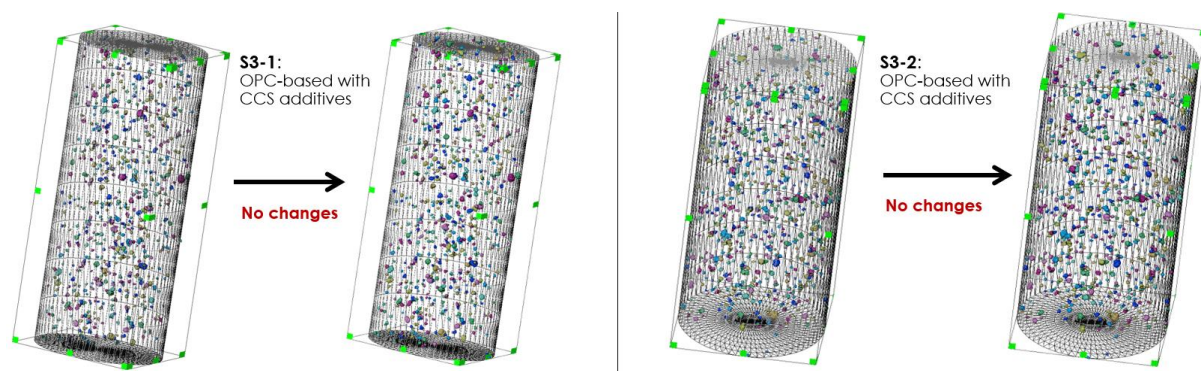


Figure 5: microstructure of samples S3-1(left) and S3-2 (right) before and after quenching. Voxel resolution of 32 μm . Samples are of sealant composition S3, OPC-based with CCS additives. There are no obvious changes after quenching in either sample.

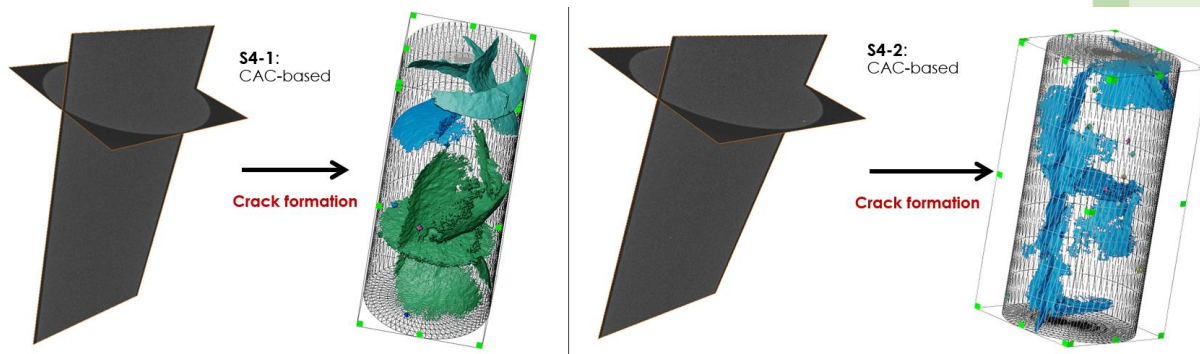


Figure 6: microstructure of samples S4-1(left) and S4-2 (right) before and after quenching. Voxel resolution of 32 μm . Samples are of sealant composition S4, CAC-based. Connected cracks and occasional new voids develop in both samples.

For sealants S1, S2, and S4 (Figures 3, 4, and 6), type 1 experiments induced cracks and voids in both samples. In sealant S1 the quenching procedure led to some connected cracks and a significant increase in void volume, and in S2 some connected cracks and some new voids were created. Sample S4 shows sample-size connected cracks, and only a few disconnected new voids after quenching. This means quenching generated sufficient thermal stresses to cause cracking in the cement of these three compositions. By quenching, multiple cracks and new voids developed at different orientations and locations throughout the sample, where in sample S4-2 (Figure 6) all thermally-induced cracks are connected to form a potential leakage pathway for flow. Note that both S4 samples are still cohesive after quenching, despite the sample-size connected cracks. On the contrary, both samples of S3 are intact after quenching, and show no obvious changes.

Figure 7 shows the structure of voids and cracks in samples of all four sealant compositions before and after type 2 flow-through experiments. Type 2 experiments also induced cracks and new voids in samples of sealants S1, S2, and S4. However, compared to quenching, only limited cracks (all radial) were created in these sealants by flow-through. These radial cracks all intersect with the borehole of the sample. In sample S1-3, the flow-through procedure created two major radial cracks and significant new voids. In sample S2-3, only one radial crack close to the injection inlet and some voids were created. And in sample S4-3, a sample-size radial crack and few voids developed after the experiment. Like in quenching for sample S4-2, flow-through created cracks also all through sample S4-3. In contrast, the flow-through procedure caused no obvious changes for sample S3-3.

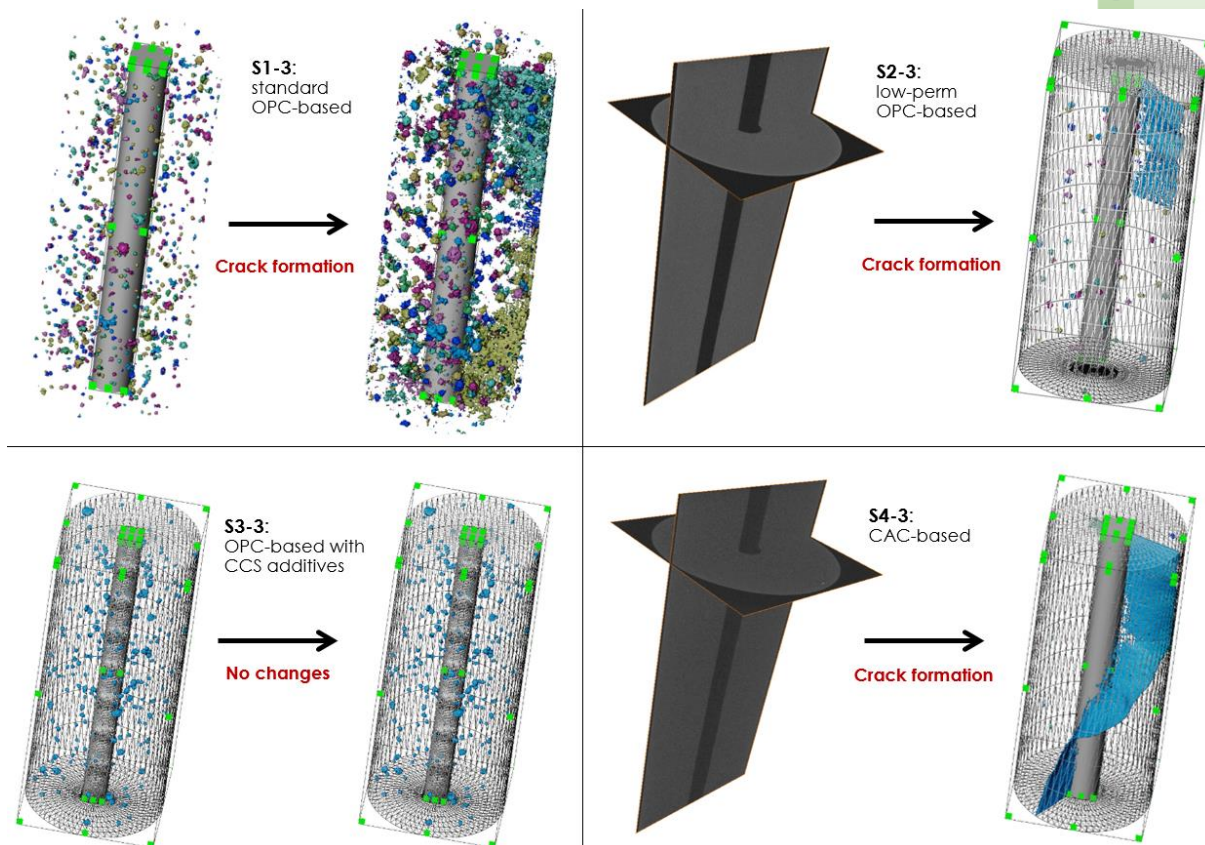


Figure 7: microstructure of samples S1-3 (sealant S1, upper left), S2-3 (sealant S2, upper right), S3-3 (sealant S3, bottom left), and S4-3 (sealant S4, bottom right) before and after flow-through experiments. Voxel resolution of 32 μm . The injection inlet is at top, and outlet at bottom of these four sample illustrations. Radial cracks and new voids develop in sealant types S1, S2 and S4, whereas in sample S4-3 the crack is sample size. Sealant S3 shows no obvious changes after the flow-through experiment.

To study quantitatively to what extent thermal-shocking experiments (both type 1 and type 2) affect sealant samples, we use Avizo software to calculate the volume of the cracks and voids in the samples (see Appendix for detailed workflow). Figure 8 compares this volume for each sample of the four sealant compositions before and after the experiment. As shown in Figure 8, the volume of cracks and voids for intact samples of sealants S2 and S4 are zero, as those samples are compact with no pre-existing voids. The volume of cracks and voids increases for all samples of sealants S1, S2, and S4 after experiments, while it stays the same for S3 samples. In general, the observed volume increase for S1, S2, and S4 is bigger for type 1 quenching than for the type 2 flow-through experiments. By quenching the relatively small sample in a 6 L cold water bath, the entire outer surface of the sample experiences an extreme and instantaneous temperature difference, creating a relatively large thermal shock effect. The maximum temperature gradient from outside to inside of the sample is therefore attained, which then creates large thermal stresses to break the sample. In contrast, in flow-through experiments, we flush 160 mL cold water through the small central borehole of the sample in 2 mins during each cycle of thermal shock. The smaller surface area in contact with cold water means that the potential for thermal stresses is much lower than by quenching. Moreover, any stresses which occur are in the radial direction and located in the vicinity of the borehole. The temperature of the water also increases as it flows through the borehole. In type 2 flow-through experiments, hence, the temperature fluctuation near the inlet of the borehole is greater than that near the outlet, which implies that larger thermal stresses are created nearby the inlet. All aforementioned mechanisms explain why for S1, S2, and S4 there are more thermally-induced cracks

and voids by quenching than by flow-through. Moreover, by quenching, they are at different orientations throughout the sample, while by flow-through fewer and only radial cracks develop and intersect with the borehole in samples.

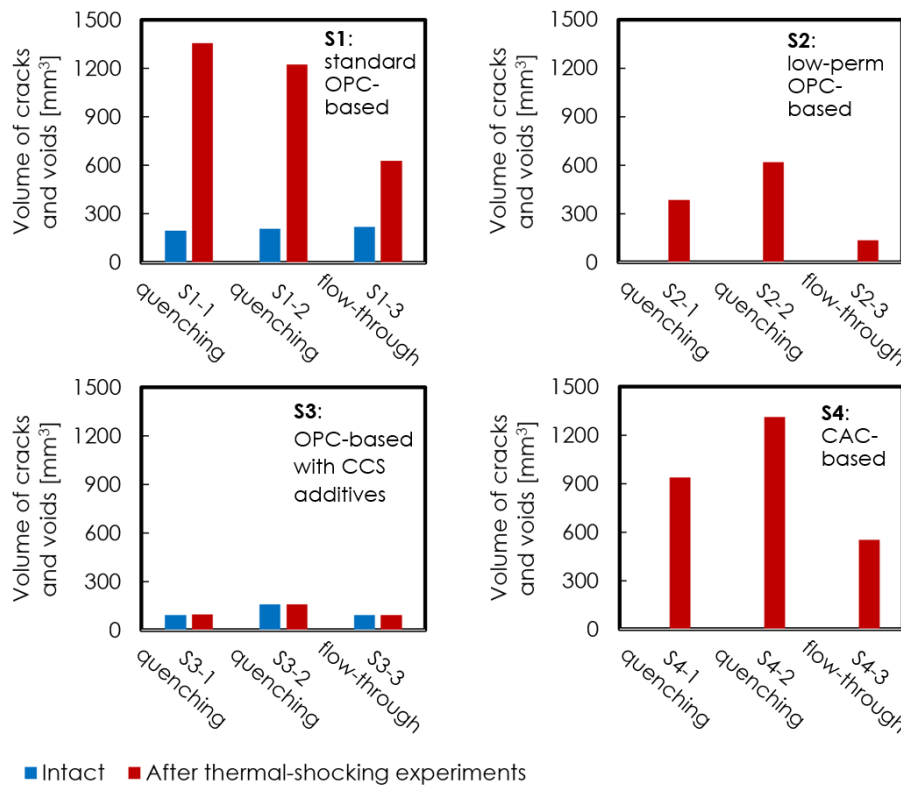


Figure 8: volume of cracks and voids for each sample of the four sealant compositions before and after thermal-shocking experiments. The volume for intact samples of sealants S2 and S4 are zero, as those samples are compact with no pre-existing voids.

3.2 Effects of thermal shocks on UCS of sealant samples

In addition, after micro-CT scanning, we measure the unconfined compressive strength (UCS) for each sample. The changes in the UCS are direct consequences of the thermal treatment. Figure 9 shows how UCS changes after thermal shocks for the four different compositions and for the two different procedures. As shown in Figure 9, the UCS of sealants S1, S2, and S4 decreases after both types of thermal-shocking experiments, where the decrease for the quenching treatment is larger than the decrease for the flow-through treatment. This is in line with the amount of damage observed for the two procedures, where the samples with a larger post-treatment crack and void volume (Figure 8) also exhibit a lower strength. The variability in UCS's for the repeat experiments is 5-11 Mpa (shown in red diamonds in Figure 9), which is much less than the difference between the intact strength and the strength after either thermal-shocking procedure. For sealants S1, S2, and S4, the reduction in UCS after quenching (by 41%, 50%, and 67% on average for S1, S2, and S4 samples, respectively) is greater than after flow-through (by 19%, 27%, and 40% for samples S1-3, S2-3, and S4-3, respectively). This relates to the changes in the volume of cracks and voids due to thermal shocks (Figure 8): for each sealant, the larger increase in the volume of thermal-induced cracks and voids leads to a greater reduction in strength. Furthermore, for sealant S3, there is no substantial change in the UCS after thermal shocks by flow-through (see S3-3 in Figure 9). Counter-intuitively, samples S3-1 and S3-2 become on average 47% stronger after quenching.

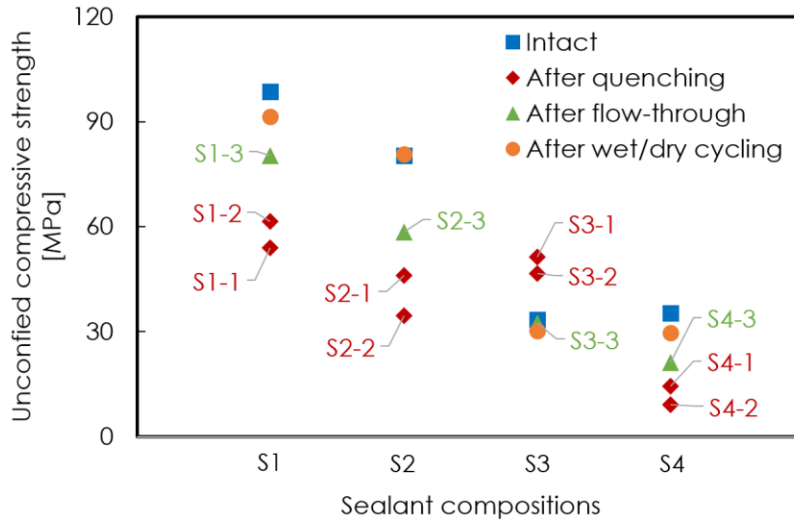


Figure 9: UCS of samples of the four sealant compositions before and after thermal-shocking experiments.

Figure 9 also displays the UCS's of samples of the four different compositions after eight room temperature wet/dry cycles. The UCS shows a slight decreases for sealants S1, S3 and S4 (by 7%, 9% and 16%, respectively), whereas it shows insignificant change for sealant S2. Note that this strength loss in sealant S1 and S4 is insignificant compared to the strength loss by either quenching or flow-through experiment. After wet-dry cycling, all samples were visually intact, so no observable fractures were created.

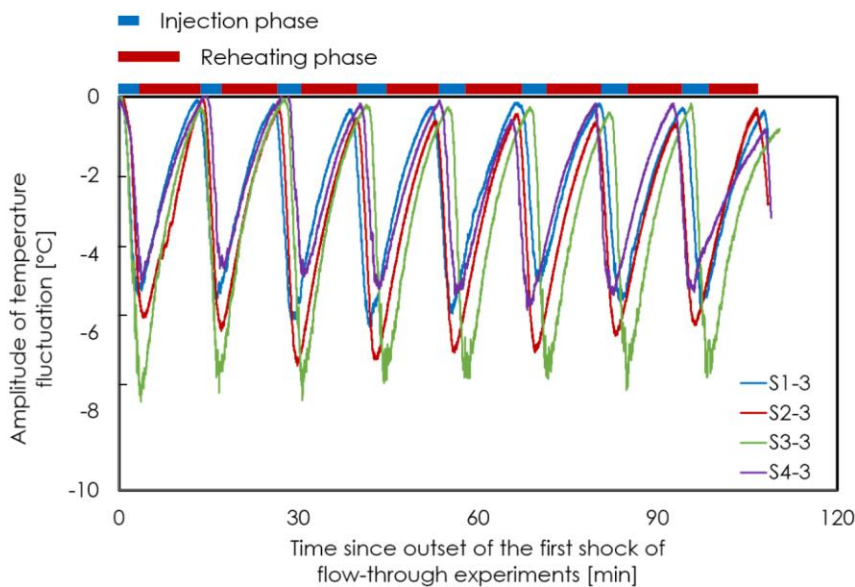


Figure 10: amplitude of temperature fluctuation during eight cycles of thermal shocks in type 2 flow-through experiments for samples of the four compositions. Time zero marks the outset of the first shock. Samples are maintained at 120°C for half an hour before time zero.

3.3 Temperature profile in type 2 experiments

During type 2 flow-through experiments, we measured the temperature, T_s , in the middle on the outer surface of the sample (Figure 2). We then use this temperature to calculate the amplitude of temperature fluctuation due to thermal shocks since the outset of the first shock (after the sample is maintained at

120°C for half an hour), by $(T_s - 120)^\circ\text{C}$. Figure 10 shows the amplitude of temperature fluctuation during the eight cycles of thermal shocks in flow-through experiments for the four samples of different compositions.

Upon each cycle of thermal shock, the temperature at the outer surface of all four samples first drops until it reaches the maximum temperature fluctuation amplitude at the end of the injection of cold water. The temperature then gradually rises back to equilibrate with the system temperature before the next shock. As the cycles progress, the samples gradually cool down where S1-3 and S4-3 usually get closest to their original temperature, followed by S3-3. S2-3 stays furthest away from the original temperature, about 0.5°C. Throughout all eight cycles of thermal shocks, the average maximum amplitude of temperature fluctuation is 5.1, 6.1, 7.4, and 4.5°C for samples S1-3, S2-3, S3-3, and S4-3, respectively.

Essentially, these temperature drops during cold-water injection phases for all four samples in type 2 experiments signify that heat has transferred from the outer part of the sample toward the central borehole. All four samples experience the same boundary conditions with respect to sample temperature prior to flow-through, the amount, temperature and the rate of injected water. Therefore, this flux of thermal energy during thermal shocks can only be governed by the thermal properties of the sealants, specifically the thermal diffusivity. Heat should transfer more rapidly in a material with a higher thermal diffusivity. Figure 11 displays the relationships between the maximum amplitude of temperature fluctuation, thermal diffusivity of samples, and the fraction of UCS reduction in type 2 flow-through experiments for the four samples. Sample S3-3 shows the highest temperature fluctuation, and the least strength reduction. It also has the highest thermal diffusivity. We postulate that due to the high thermal diffusivity less thermal stresses built up, and that therefore less damage results from high temperature fluctuations during thermal cycles. This would explain why sample S3-3 was undamaged after thermal shocks.

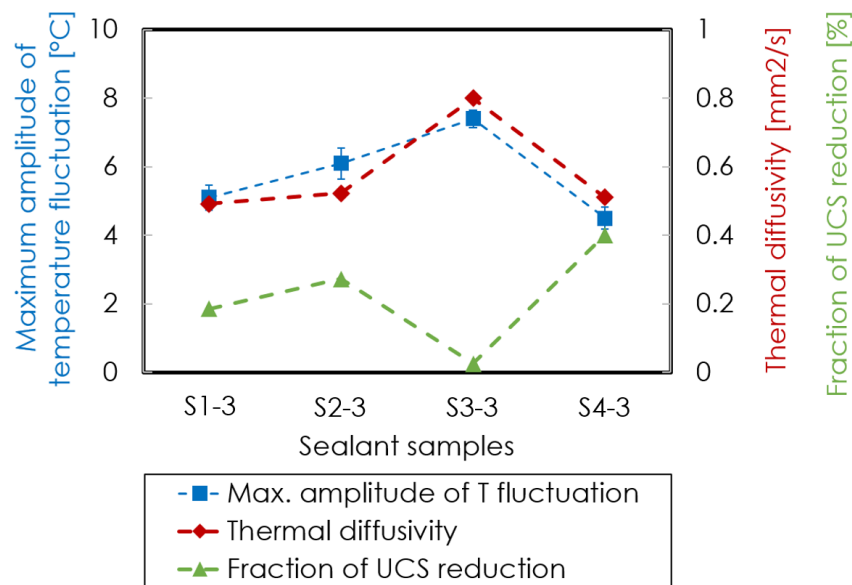


Figure 11: relationships between the maximum amplitude of temperature fluctuation, thermal diffusivity of samples, and the fraction of UCS reduction in type 2 flow-through experiments for the four samples of different compositions.

4 Discussion

In this study, we tested sealant samples of four compositions to study their integrity under thermal shocks for CCS applications. In our study, in addition to two reference OPC-based sealants (S1 and S2), we also tested two blends with different compositions designed for future CCS wells (S3 and S4). S3 is based on OPC but with CO₂-sequestering additives, and its integrity was not compromised after the flow-through

experiment, and even enhanced after quenching. Despite the high curing temperature and pressure, we speculate that the enhancements during quenching resulted from thermally-provoked chemical reactions. Sealant S4 is based on calcium aluminate cement (CAC), and all S4 samples fully lost integrity after both types of thermal shocks. Compared to OPC, CAC contains a far greater amount of alumina (>90%) and a far less amount of silica (Barborak, 2010). Even though CAC gains significantly higher early strength during its curing process, it may undergo a conversion process later where a strength loss of 50% or more is possible. This process happens when metastable phases of the hydration products convert to more stable ones. We speculate that it is possible that the thermal treatment speeds up this conversion.

All experiments were conducted at a worst-case scenario with zero confinement, whereas at CO₂ storage depths we expect cement to experience a confining pressure up to 10 MPa (10 km depth, Kirby et al., 2001; Alnes et al., 2011; Zhang et al., 2022). In such a case, the presence of confinement should avoid or at least mitigate the adverse effects of thermal stresses on cement integrity. The confinement is expected to provide support to the sealant sample and increase its stiffness, hence reducing the potential for thermally-induced cracks in the cement. This would be in line with what De Andrade et al. (2015) have found before for annuli between casing, cement and rock undergoing thermal cycles.

Our samples started out dry, and became progressively more water-saturated with each thermal shock. However, our wet-dry cycling reference experiments showed that the integrity compromise for sealants S1, S2 and S4 by both types of thermal-shocking experiments is substantial compared to any mechanochemical changes due to water exposure alone. Torsæter et al. (2017) studied the integrity at the interface between cement and rock by applying thermal shocks to the sample with liquid nitrogen. They found that a dried sample remained intact and a wet sample lost its integrity after thermal shocks. Yet it is still not clear how wet samples of our sealant compositions behave under thermal shocks. This topic deserves further study.

5 Conclusions

In this study, we conducted two types of experiments to investigate the type and extent of thermal damage and what its effects are on the integrity of sealants of four different compositions. These sealants include reference OPC-based blends (S1, based on standard OPC, and S2, based on OPC with ultra-low permeability), newly-designed blend (S3, based on OPC with CO₂-sequestering additives), and CAC-based blend (S4).

We found that samples of sealants S1, S2, and S4 lost their integrity after both types of thermal-shocking experiments, indicating that these compositions may not be optimal candidates for well-sealing materials for CCS. For all these three sealants, quenching displayed more jeopardizing effects than flow-through experiments. By quenching, cracks and new voids developed throughout the samples at different orientations and caused a decrease in UCS by 41%, 50%, and 67% on average for samples of S1, S2, and S4 compositions, respectively. In flow-through experiments, only a limited number of radial cracks that intersected with the borehole, and voids were initiated. UCS decreases by 19%, 27%, and 40% for S1, S2, and S4 samples, respectively. This is because, by quenching, a larger surface of the sealants was exposed to a high temperature difference, i.e. creating a more severe thermal shock. In such a case, greater thermal stresses were accumulated which resulted in larger adverse effects on sealant integrity.

However, we have not observed any thermally-induced cracks in samples of sealant S3 after experiments. The flow-through experiment caused no significant changes in the S3 sample, and quenching even somewhat enhanced the integrity of this sealant with an increase in strength. We postulate that this is caused by the higher thermal diffusivity of sealant S3 compared to the other three sealants. The increased efficiency of heat transfer throughout the sample led to lower thermal stresses, insufficient to damage the integrity of S3 samples.

Our study implies that standard OPC-based sealants used in most of the currently existing wells and the CAC-based sealant designed for future CCS wells are prone to failure under strong thermal shocks

encountered during cyclic CO₂ injection and storage afterward. Upgrading sealant materials to prevent or mitigate the adverse effects of thermal shocks and maintain long-term wellbore sealing integrity during CCS can be beneficial.

In short, this study provides a novel method to study existing and newly-designed sealants, and assess their integrity under strong thermal shocks in a worst-case scenario i.e. dry samples without confinement. Based on these results, we observed different thermally-induced cracking behaviors for sealants of different compositions, where we postulate that their thermal diffusivity is the key characteristic that determines the capacity of sealants to maintain integrity under thermal shocks.

Acknowledgement:

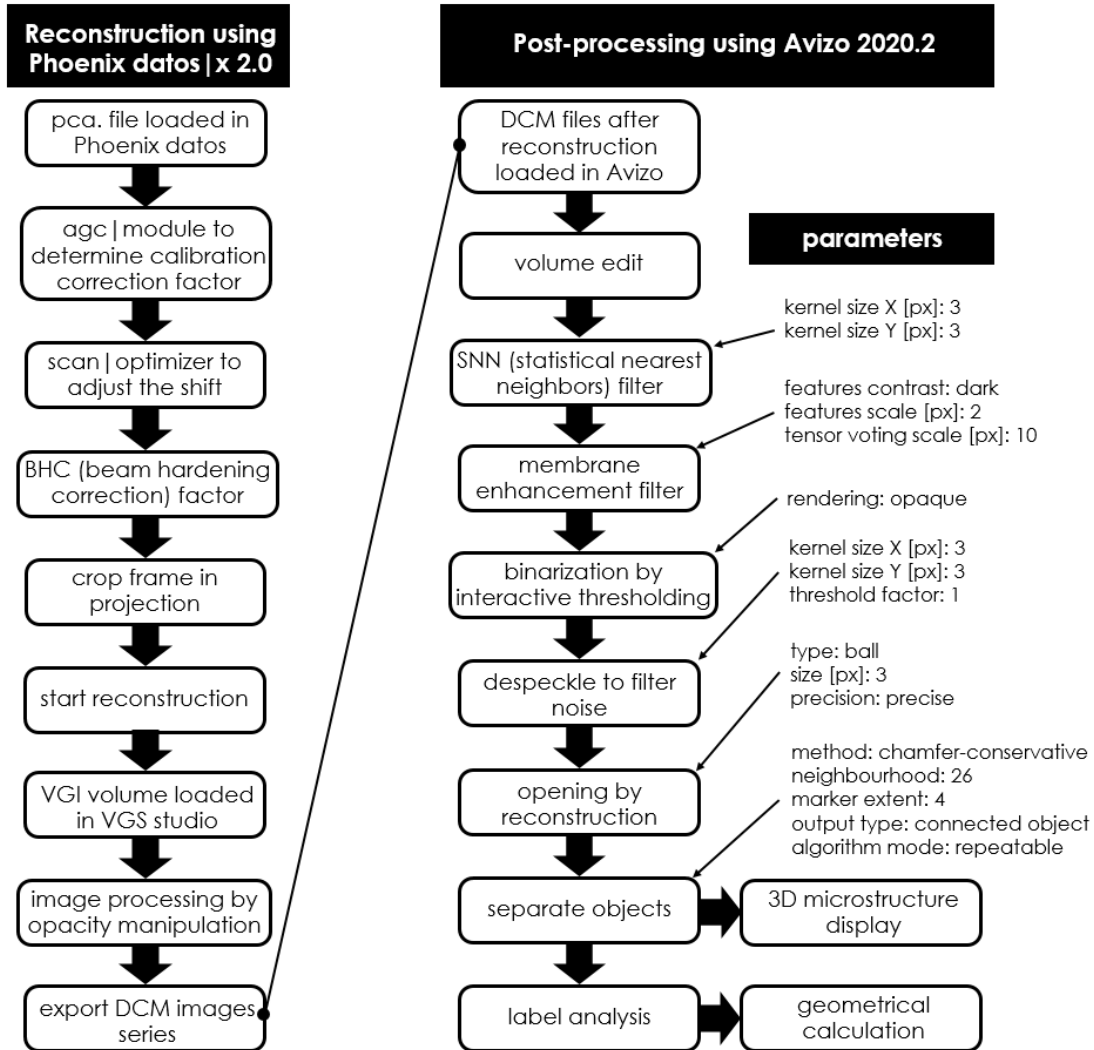
The CEMENTTEGRITY project is funded through the ACT program (Accelerating CCS Technologies, Horizon2020 Project No 691712).

Financial contributions from the Research Council of Norway (RCN), the Netherlands Enterprise Agency (RVO), the Department for Energy Security & Net Zero (DESNZ, UK), and Harbour Energy are gratefully acknowledged.



Appendix

In this study, we use Phoenix datos software to post-process the images of each sample acquired by micro-CT scanning. We then use Avizo software to construct the 3D microstructure of cracks and voids in the sample. The workflow is shown below.



References

- Albawi, A., De Andrade, J., Torsæter, M., Opedal, N., Stroisz, A., & Vrålstad, T. (2014, February). Experimental set-up for testing cement sheath integrity in arctic wells. In *OTC Arctic Technology Conference*. OnePetro.
- Alnes, H., Eiken, O., Nooner, S., Sasagawa, G., Stenvold, T., & Zumberge, M. (2011). Results from Sleipner gravity monitoring: Updated density and temperature distribution of the CO₂ plume. *Energy Procedia*, **4**, 5504-5511.
- Barborak, R. (2010). Calcium aluminate cement concrete (class cac concrete) txdot special specification ss-4491 tip sheet. Construction and Bridge Divisions, Texas Department of Transportation: Austin, TX, USA.
- Budinis, S., Krevor, S., Mac Dowell, N., Brandon, N., & Hawkes, A. (2018). An assessment of CCS costs, barriers and potential. *Energy strategy reviews*, **22**, 61-81.
- Bui, M., Adjiman, C. S., Bardow, A., Anthony, E. J., Boston, A., Brown, S., ... & Mac Dowell, N. (2018). Carbon capture and storage (CCS): the way forward. *Energy & Environmental Science*, **11**(5), 1062-1176.
- Carey, J. W., Wigand, M., Chipera, S. J., WoldeGabriel, G., Pawar, R., Lichtner, P. C., Wehner, S. C., Raines, M. A., & Guthrie Jr, G. D. (2007). Analysis and performance of oil well cement with 30 years of CO₂ exposure from the SACROC Unit, West Texas, USA. *International journal of greenhouse gas control*, **1**(1), 75-85.
- Carpenter, R. B., Brady, J. L., & Blount, C. G. (1992). The effects of temperature and cement admixes on bond strength. *Journal of Petroleum Technology*, **44**(08), 936-941.
- Celia, M. A., Bachu, S., Nordbotten, J. M., Gasda, S. E., & Dahle, H. K. (2005). Quantitative estimation of CO₂ leakage from geological storage: Analytical models, numerical models, and data needs. In *Greenhouse Gas Control Technologies 7* (pp. 663-671). Elsevier Science Ltd.
- De Andrade, J., Sangesland, S., Todorovic, J., & Vrålstad, T. (2015, April). Cement sheath integrity during thermal cycling: a novel approach for experimental tests of cement systems. In *SPE Bergen one day seminar*. OnePetro.
- Dugonjic-Bilic, F., Tiemeyer, C., & Plank, J. (2011, April). Study on admixtures for calcium aluminate phosphate cement useful to seal CCS wells. In *SPE International Symposium on Oilfield Chemistry*. OnePetro.
- Eiken, O., Ringrose, P., Hermanrud, C., Nazarian, B., Torp, T. A., & Høier, L. (2011). Lessons learned from 14 years of CCS operations: Sleipner, In Salah and Snøhvit. *Energy procedia*, **4**, 5541-5548.
- Haszeldine, R. S. (2009). Carbon capture and storage: how green can black be?. *Science*, **325**(5948), 1647-1652.
- Kirby, G. A. (2001). Depth Mapping and Characterisation of the Utsira Sand Saline Aquifer, Central and Northern North Sea: *British Geological Survey Report CR/01/218N*. British Geological Survey.
- Lescanne, M., Hy-Billiot, J., Aimard, N., & Prinet, C. (2011). The site monitoring of the Lacq industrial CCS reference project. *Energy Procedia*, **4**, 3518-3525.
- Lesti, M., Tiemeyer, C., & Plank, J. (2013). CO₂ stability of Portland cement based well cementing systems for use on carbon capture & storage (CCS) wells. *Cement and concrete research*, **45**, 45-54.
- Lund, H., Torsæter, M., & Munkejord, S. T. (2015, April). Study of thermal variations in wells during CO₂ injection. In *SPE Bergen One Day Seminar*. OnePetro.
- Metz, B., Davidson, O., De Coninck, H. C., Loos, M., & Meyer, L. (2005). IPCC special report on carbon dioxide capture and storage. Cambridge: Cambridge University Press.
- Neville, A. M., & Brooks, J. J. (1987). *Concrete technology* (Vol. 438). England: Longman Scientific & Technical.
- Parker, M. E., Meyer, J. P., & Meadows, S. R. (2009). Carbon dioxide enhanced oil recovery injection operations technologies. *Energy Procedia*, **1**(1), 3141-3148.
- Roy, P., Walsh, S. D., Morris, J. P., Iyer, J., Hao, Y., Carroll, S., ... & Torsæter, M. (2016, June). Studying the impact of thermal cycling on wellbore integrity during CO₂ injection. In *50th US Rock Mechanics/Geomechanics Symposium*. OnePetro.

Samara, H., Al-Eryani, M., & Jaeger, P. (2022). The role of supercritical carbon dioxide in modifying the phase and interfacial properties of multiphase systems relevant to combined EOR-CCS. *Fuel*, **323**, 124271.

Santra, A., & Sweatman, R. (2011). Understanding the long-term chemical and mechanical integrity of cement in a CCS environment. *Energy Procedia*, **4**, 5243-5250.

Selma, L., Seigo, O., Dohle, S., & Siegrist, M. (2014). Public perception of carbon capture and storage (CCS): A review. *Renewable and Sustainable Energy Reviews*, **38**, 848-863.

Torsæter, M., Todorovic, J., Lavrov, A., Gawel, K., Lund, H., Roy, P., & Carroll, S. (2017). Avoiding damage of CO₂ injection wells caused by temperature variations. *Energy Procedia*, **114**, 5275-5286.

Vilarrasa, V., & Rutqvist, J. (2017). Thermal effects on geologic carbon storage. *Earth-science reviews*, **165**, 245-256.

Yoo, B. Y., Choi, D. K., Kim, H. J., Moon, Y. S., Na, H. S., & Lee, S. G. (2013). Development of CO₂ terminal and CO₂ carrier for future commercialized CCS market. *International Journal of Greenhouse Gas Control*, **12**, 323-332.

Zhang, K., Lau, H. C., & Chen, Z. (2022). Extension of CO₂ storage life in the Sleipner CCS project by reservoir pressure management. *Journal of Natural*